ISMRM 2015 Educational Session - RF Engineering: Coils

Multi-Tuned RF Coils

Ryan Brown[1,2]
ryan.brown@nyumc.org

[1]Center for Advanced Imaging Innovation and Research (CAI²R) and [2]Bernard and Irene Schwartz Center for Biomedical Imaging, Department of Radiology, New York University School of Medicine, New York, NY USA

Highlights

- Dual-tuned coils provide co-registered anatomical images and B_0 shim settings (^{1}H module) and metabolic information (x-nuclei module) without repositioning the subject or coil
- X-nuclei signal strength is typically less than 1/1,000× that of ^{1}H (1) → A dual-tuned coil must maximize x-nuclei receive sensitivity while simultaneously providing adequate ^{1}H sensitivity
- We will discuss prevalent dual-tuning techniques and considerations for performance characterization and interfacing the coil

Background

Multi-nuclear MRI and MRS are of great interest to the scientific community because of the ability to probe functional metabolites such as ^{23}Na, ^{31}P, ^{19}F, ^{7}Li, ^{13}C, ^{129}Xe, etc., which are collectively referred to as "x-nuclei." For example, quantitative ^{23}Na MRI has been shown to be highly specific to the glycosaminoglycan content in cartilage and could therefore be used as a means of detection and assessment of the degree of biochemical degradation of cartilage in the early stages of osteoarthritis. Meanwhile, ^{31}P MRS can quantify metabolites that play important roles in energy consumption in the skeletal muscle, heart, liver, and brain.

A dual-nuclei RF coil is preferred for x-nuclei applications; the ^{1}H module provides anatomical reference images and B_0 shim settings, while the x-nuclei module provides metabolic information without repositioning the subject or coil hardware. Given that standard RF coils are narrowband devices tuned only to the ^{1}H frequency, specialized techniques must be used to *simultaneously* provide sensitivity at both the ^{1}H and x-nuclei frequencies of interest (Table 1). Popular techniques for achieving dual resonance will be reviewed in the following section.

Table 1. Gyromagnetic ratio and NMR signal strength in the human brain for common nuclei.

Nucleus	^{1}H	^{31}P	^{7}Li	^{23}Na	^{13}C
$\gamma/2\pi$ (MHz/T)	42.576	17.235	16.546	11.262	10.705
Signal relative to ^{1}H	1	1×10^{-5}	3×10^{-6}	5×10^{-5}	4×10^{-10}

It is important to keep in mind that the main difficulty with x-nuclei MRI is its fundamentally low signal-to-noise ratio (SNR) due primarily to the low concentration of x-nuclei in the body, which is reflected in values in the last row of Table 1. This often implies undesirably long acquisition times and large voxel volumes. Over the past several years, the SNR deficit has been somewhat alleviated by the development of efficient pulse sequences and reconstruction techniques along with the proliferation of high field scanners (≥ 3 Tesla). SNR advances have also been achieved with recent dual-nuclei RF coil designs, which have transitioned from preceding single channel and volume coils to multi-element phased arrays. Multi-element phased arrays are advantageous because they combine the large field-of-view of a volume coil with the improved sensitivity of a surface coil (2,3).

Proc. Intl. Soc. Mag. Reson. Med. 23 (2015)

Dual-Nuclei Coil Methods

Single tuned coil

A coil's inherent inductive impedance is given by $Z_L = j\omega L$. A single resonance is achieved by canceling the inductance with a tuning capacitor $Z_T = (j\omega C)^{-1}$ such that $Z = j\omega L + (j\omega C)^{-1} = 0$. Plots of the coil's negative inductive reactance and tuning network reactance curves show that resonance occurs at their intersection at the x-nuclei frequency (Figure 1).

Pole insertion

One way to achieve dual resonance is by inserting a pole in the form of a parallel inductor/capacitor pair, or "trap" circuit, in series with the coil (4-6). In this case, the tuning network impedance is $Z_{T'} = (j\omega C')^{-1} + \frac{j\omega L_p (j\omega C_p)^{-1}}{j\omega L_p + (j\omega C_p)^{-1}}$. Inspection of the reactance plot shows two intersections between the coil's negative inductive reactance and tuning network, which correspond to resonances at both ^{1}H and x frequencies. The low resonance frequency can be modified primarily by the main capacitance *C'*, while the high resonance frequency can be modified primarily by the pole capacitance C_p. In general, dual-nuclei coil techniques involve tradeoffs. In the pole insertion method, flux generated in the trap inductor L_p is not coupled to the sample and therefore generates loss associated with its resistance. The efficiency of the low frequency channel approaches unity (where unity is the baseline efficiency of a single tuned coil) when the value of L_p approaches zero. In practice, the ratio of L_p:L is chosen to be ~1:4-5, yielding ~90% efficiency on the low frequency channel and ~45% efficiency on the high frequency channel (4).

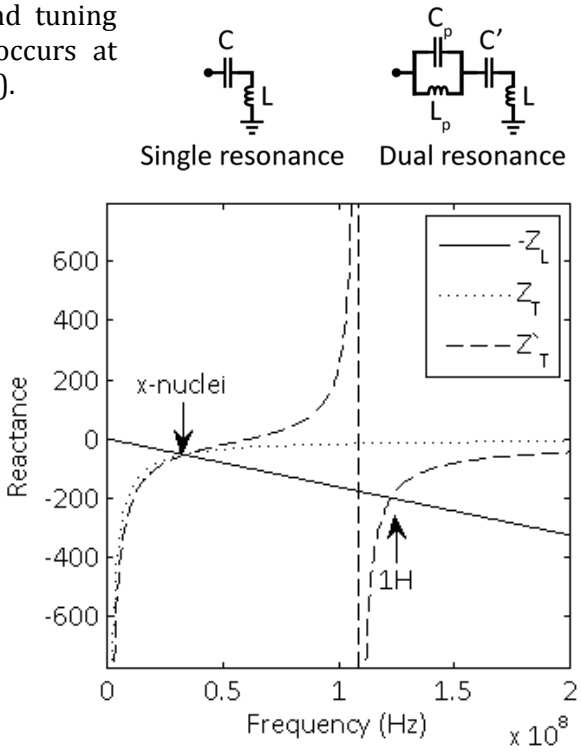

Figure 1. Schematic diagram of a single-tuned coil and dual-tuned "trap" coil (top) and their reactance curves (bottom). In this example, the x-nuclei and ^{1}H resonances occurs at 32.6 MHz and 123MHz, corresponding to ^{23}Na/^{1}H at 3 Tesla.

Other methods – nested, transformer coupled, etc.

Another method to achieve dual resonance is to use two separate "nested" or explicitly coupled transformer coils, whose individual structures can be semi-independently tuned to the low and high frequencies of interest (7-22). In this case, it is instructive to look at the behavior of each coil at both frequencies. Again, the reactive portion of the coil impedance is given by $Z = j\omega L + (j\omega C)^{-1}$. Consider a coil that is tuned to the proton frequency: $Z(\omega = \omega_{1\mathrm{H}}) = 0$. When viewed at the lower x-nucleus frequency, its impedance is dominated by a large capacitive reactance and therefore approximates an open circuit: $Z(\omega = \omega_{low}) \sim (j\omega_{low}C)^{-1} \rightarrow \infty$. Of course, the degree to which the ^{1}H coil approaches the open circuit condition is proportional to the ratio between the resonant frequencies of interest. Consider next a coil tuned to the x-nuclei frequency $Z'(\omega = \omega_{low}) = 0$. When viewed at the proton frequency, its impedance is dominated by its inherent inductive reactance and therefore can be thought of as a shield: $Z'(\omega = \omega_{1\mathrm{H}}) \sim j\omega_{1\mathrm{H}}L$. This combination of behaviors can be leveraged in a concentric nested dual nuclei strategy; 1) the outer low frequency coil is not significantly affected by the inner high frequency coil, while 2) the low frequency coil shields the high frequency coil to reduce its radiation loss and neighbor coupling (23), albeit at the

expense of coverage and penetration due to counter-rotating current induced in the low frequency coil shield. ^{1}H traps can reduce counter-rotating currents in the x-nuclei coil with a small penalty on x-nuclei SNR (21,22). Another method to reduce counter-rotating currents is with a ^{1}H butterfly/x-nuclei loop pair, which generate orthogonal fields and hence experience very little coupling (19,20). This approach can be desirable in proton decoupling applications, where a so-called B_2 field is generated to saturate ^{1}H spins concurrent to the x-nuclei MRS experiment to augment the x-nuclei signal.

Still other dual-nuclei coil techniques have included modified volume coils with alternating ^{1}H/x legs (24-26) and additional endrings (27,28). Volume coils generally provide a uniform transmit field (B_1^+), which can simplify x-nuclei quantification methods that may be sensitive to a spatially varying flip angle.

Dual-tuned phased arrays

While early dual-tuned coils primarily consisted of single channel surface or volume coils, recent literature shows a dramatic increase in dual-tuned phased arrays (8,10,11,13,14,16,17). This can be traced to a general revitalization of x-nuclei research resulting from higher magnetic fields and improved pulse sequences and sampling strategies. Ideally, many-element arrays outperform single channel coils in both the periphery as well as in the center of the object (3). However, transitioning from a single channel x-nuclei coil to a many-element array implies a diminishing quality factor $\left(Q = \frac{f_0}{BW} = \frac{\omega L}{R}\right)$ ratio that coincides with smaller coils. A good rule-of-thumb is to design the quantity and size of the array elements such that the required coverage is provided and each element has a Q ratio ≥ ~3, which is considered to be on the edge of the sample noise dominated regime (an array with a higher channel count but lower Q ratio is unlikely to provide SNR benefit). Further, higher channel counts necessitate additional opportunities for unwanted stray currents and noise coupling (i.e. through coaxial cables, interface components, and preamplifiers). Subtle enhancements such as presenting the preamplifier with an impedance mismatch can reduce noise coupling between coils, which can be particularly beneficial in x-nuclei arrays where the loaded Q is high due to low coil-tissue coupling (10,29,30).

Performance characterization

As is the case for single tuned coils, it is important to quantify dual-tuned coil performance. The quality factor is a straightforward way to measure coil efficiency; the unloaded Q_U is an indication of losses associated with the coil itself (namely conductor resistance and radiation) and the loaded Q_L is an indication of losses in the coil plus those induced from the sample. Here, coil Q was measured on ^{31}P/^{1}H coils tuned for operation at 7 Tesla as a means to compare several dual-nuclei strategies in Figure 2.

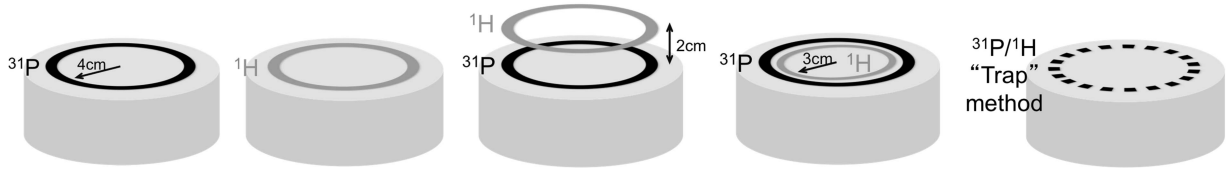

	^{31}P Isolated	^{1}H Isolated	^{31}P/^{1}H Offset	^{31}P/^{1}H Concentric	^{31}P/^{1}H Trap*
	Q_U/Q_L				
^{31}P	440/34	---	447/33	418/31	346/35
^{1}H	---	245/9	270/105	315/47	190/67

Figure 2. Q measurements for a variety of single and dual-tuned coil configurations. * L_p:L ≈ 1:5.

Several interesting conclusions can be drawn from the Q measurements. Importantly, the Q of the ^{31}P coil is practically unaffected by the presence of the ^{1}H coil in the offset and concentric arrangements. Conversely, the offset ^{31}P coil shields the ^{1}H coil, resulting in an increased unloaded Q value (due to reduced radiation loss) but also a much higher loaded Q due to shielding of the coil from the sample and thus a significantly reduced Q ratio. The concentric arrangement partially restores the Q ratio of the ^{1}H coil, while the trap method results in loss of performance at both frequencies.

The key performance metric in a dual-tuned coil is the SNR of the x-nuclei module. It can be insightful to compare the SNR of a coil developed in-house to that attained with a commercially available coil that serves as a reference standard. When a reference coil is not available, it can be problematic to engage in inter-site SNR comparison owing to the wide variety of specialized pulse sequences and acquisition parameters and the arbitrary nature of SNR units. For this reason, it is preferred to publish SNR measurements acquired with standard gradient echo Cartesian sequences and a well-described phantom such that the measurements can be easily replicated at other institutions.

A performance metric that is somewhat easier to quantify is transmit efficiency. This quantity stipulates the amount of power or voltage required to generate a given B_1^+. Various flip angle mapping methods can be applied to determine ^{1}H transmit efficiency. However, x-nuclei flip angle mapping methods are generally not available. One approach, although time-consuming, is to acquire fully relaxed gradient echo images (TR>>T1) over a range of transmit pulse amplitudes V with known duration τ. The signal intensities can then be fit to a sine curve to determine the pulse amplitude required to generate a flip angle α. This value can finally be translated into transmit efficiency: $\eta = B_1^+/V = \frac{360}{\alpha}\gamma\tau/V$, which is a convenient metric for coil comparisons due to its relative insensitivity to imaging parameters.

Interface

Due to the lack of an x-nuclei transmit coil (the body coil in clinical magnets operates only at the ^{1}H frequency), dual-nuclei coils are typically operated in transmit/receive mode or transmit only/receive only (ToRo) mode, both of which necessitate custom transmit/receive switches and other interface hardware (31). Additionally, coils designed with proton decoupling applications in mind require a low-loss low-pass or band-pass filter at the input of the x-nuclei preamplifier to prevent damage from power leaked from the relatively large concurrent ^{1}H B_2 pulses.

Cable traps are essential components that reduce common mode currents on the coaxial cable shields in any RF coil (32). In particular, electric fields generated on coaxial cables in close proximity to the subject can pose a safety hazard, while their existence generally deteriorates coil performance. In dual-tuned coils, cable traps are typically required to suppress both ^{1}H and x-nuclei current, regardless of the resonant frequency of the coil connected to a given cable. Dual-tuned cable traps can be formed in a similar manner (i.e. using trap circuits) as a dual-tuned coil is formed; an excellent example of a dual-tuned tri-axial cable trap is detailed in Ref. (13).

Power Limits

Dual-nuclei transmit coils must be carefully regulated in order to restrict tissue heating caused by their electric field in accordance with limits set by the International Electrotechnical Commission (IEC 60601-2-33 2010). The merits of various approaches for determining safe power limits for RF coils are a topic of vigorous discussion in the field. Computer-based specific absorption rate (SAR) prediction models provide excellent insight on the coil's behavior, though extreme care must be taken to accurately represent the coil, relevant interface components, and subject in the computer model and finally confirm their equivalence (33,34). In the case of dual-nuclei coils, it is important to model and simulate both ^{1}H and x-nuclei coil structures to account for their interaction and to

determine power limits for both operating frequencies. An accompanying approach is to measure heating *in situ* through MR thermometry (35) and/or fluoroptic probes. The main benefit of this approach is that all components of the RF chain are inherently accounted for, although it is critical to recognize experimental subtleties such as the heat diffusivity of the phantom and B_0 drift that can reduce accuracy. Given the uncertainties associated with both simulation and thermometry methods, it is generally prudent to install a safety margin beyond the IEC limits.

Summary

Dual-nuclei coils are valuable tools for x-nuclei studies whose performance plays a critical role in improving image quality while minimizing acquisition time and spatial resolution. Many of the sound engineering guidelines for single-tuned coils such as minimizing coil loss, improving sensitivity through multi-element receive structures, and eliminating coaxial cable shield currents can be extended to dual-nuclei coils. Dual-resonance can be achieved in a variety of manners, all of which are intended to maximize receive sensitivity on the x-nuclei module while simultaneously providing adequate ^{1}H sensitivity. The popular techniques mentioned above can be considered a starting point for those interested in designing multi-tuned coils.

References

1. Haacke EM, Brown RW, Thompson MR, Venkatesan R. Magnetic Resonance Imaging - physical principles and sequence design. New York: Wiley-Liss; 1999.
2. Roemer PB, Edelstein WA, Hayes CE, Souza SP, Mueller OM. The NMR phased array. Magn Reson Med 1990;16(2):192-225.
3. Wright SM, Wald LL. Theory and application of array coils in MR spectroscopy. NMR Biomed 1997;10(8):394-410.
4. Schnall MD, Subramanian VH, Leigh JS, Chance B. A new double-tuned probe for concurrent 1H and 31P NMR. J Magn Reson 1985;65:122-129.
5. Shen GX, Boada FE, Thulborn KR. Dual-frequency, dual-quadrature, birdcage RF coil design with identical B1 pattern for sodium and proton imaging of the human brain at 1.5 T. Magn Reson Med 1997;38(5):717-725.
6. Shen GX, Wu JF, Boada FE, Thulborn KR. Experimentally verified, theoretical design of dual-tuned, low-pass birdcage radiofrequency resonators for magnetic resonance imaging and magnetic resonance spectroscopy of human brain at 3.0 Tesla. Magn Reson Med 1999;41(2):268-275.
7. Fitzsimmons JR, Brooker HR, Beck B. A transformer-coupled double-resonant probe for NMR imaging and spectroscopy. Magn Reson Med 1987;5(5):471-477.
8. Brown R, Madelin G, Lattanzi R, Chang G, Regatte RR, Sodickson DK, Wiggins GC. Design of a nested eight-channel sodium and four-channel proton coil for 7T knee imaging. Magn Reson Med 2013;70(1):259-268.
9. Fleysher L, Oesingmann N, Brown R, Sodickson DK, Wiggins GC, Inglese M. Noninvasive quantification of intracellular sodium in human brain using ultrahigh-field MRI. NMR Biomed 2013;26(1):9-19.
10. Brown R, Lakshmanan K, Madelin G, Chang G, Sodickson DK, Regatte RR, Wiggins GC. Design and Application of a Nested Multi-Channel Sodium Proton Knee Array at 3T. ISMRM. Milan, Italy2014. p 4880.
11. Lakshmanan K, Brown R, Madelin G, Boada FE, Wiggins G. An 8 channel transmit receive sodium & nested 8 channel transmit receive proton coil for 3.0 T brain imaging. ISMRM. Milan, Italy2014.
12. Fitzsimmons JR, Beck BL, Brooker HR. Double resonant quadrature birdcage. Magn Reson Med 1993;30(1):107-114.

13. Avdievich NI, Hetherington HP. 4 T Actively detuneable double-tuned 1H/31P head volume coil and four-channel 31P phased array for human brain spectroscopy. J Magn Reson 2007;186(2):341-346.
14. Moon CH, Kim JH, Zhao T, Bae KT. Quantitative (23) Na MRI of human knee cartilage using dual-tuned (1) H/(23) Na transceiver array radiofrequency coil at 7 tesla. J Magn Reson Imaging 2013;38(5):1063-1072.
15. Klomp DW, van de Bank BL, Raaijmakers A, Korteweg MA, Possanzini C, Boer VO, van de Berg CA, van de Bosch MA, Luijten PR. 31P MRSI and 1H MRS at 7 T: initial results in human breast cancer. NMR Biomed 2011;24(10):1337-1342.
16. van der Velden TA, Italiaander M, van der Kemp WJ, Raaijmakers AJ, Schmitz AM, Luijten PR, Boer VO, Klomp DW. Radiofrequency configuration to facilitate bilateral breast P MR spectroscopic imaging and high-resolution MRI at 7 Tesla. Magn Reson Med 2014.
17. Kaggie JD, Hadley JR, Badal J, Campbell JR, Park DJ, Parker DL, Morrell G, Newbould RD, Wood AF, Bangerter NK. A 3 T sodium and proton composite array breast coil. Magn Reson Med 2014;71(6):2231-2242.
18. Bottomley PA, Hardy CJ, Roemer PB. Phosphate metabolite imaging and concentration measurements in human heart by nuclear magnetic resonance. Magn Reson Med 1990;14(3):425-434.
19. Bottomley PA, Hardy CJ, Roemer PB, Mueller OM. Proton-decoupled, Overhauser-enhanced, spatially localized carbon-13 spectroscopy in humans. Magn Reson Med 1989;12(3):348-363.
20. Adriany G, Gruetter R. A half-volume coil for efficient proton decoupling in humans at 4 tesla. J Magn Reson 1997;125(1):178-184.
21. Dabirzadeh A, McDougall MP. Trap Design for Insertable Second-Nuclei Radiofrequency Coils for Magnetic Resonance Imaging and Spectroscopy. Concepts in Magnetic Resonance Part B (Magnetic Resonance Engineering), 2009;35B(3):121-132.
22. Alecci M, Romanzetti S, Kaffanke J, Celik A, Wegener HP, Shah NJ. Practical design of a 4 Tesla double-tuned RF surface coil for interleaved 1H and 23Na MRI of rat brain. J Magn Reson 2006;181(2):203-211.
23. Lanz T, Griswold M. Concentrically Shielded Surface Coils - A New Method for Decoupling Phased Array Elements. ISMRM2006. p 217.
24. Xie Z, Xu D, Kelley DA, Vigneron DB, Zhang X. Dual-frequency Volume Microstrip Coil with Quadrature Capability for 13C/1H MRI/MRS at 7T. ISMRM Workshop on Advances in High Field MR. Pacific Grove, California, USA2007. p Poster 41.
25. Vaughan JT, Hetherington HP, Otu JO, Pan JW, Pohost GM. High frequency volume coils for clinical NMR imaging and spectroscopy. Magn Reson Med 1994;32(2):206-218.
26. Amari S, Ulug AM, Bornemann J, van Zijl PC, Barker PB. Multiple tuning of birdcage resonators. Magn Reson Med 1997;37(2):243-251.
27. Murphy-Boesch J, Srinivasan R, Carvajal L, Brown TR. Two configurations of the four-ring birdcage coil for 1H imaging and 1H-decoupled 31P spectroscopy of the human head. J Magn Reson B 1994;103(2):103-114.
28. Lanz T, von Kienlin M, Behr W, Haase A. Double-tuned four-ring birdcage resonators for in vivo 31P-nuclear magnetic resonance spectroscopy at 11.75 T. Magma 1997;5(3):243-246.
29. Vester M, Biber S, Rehner R, Wiggins G, Brown R, Sodickson D. Mitigation of Inductive Coupling in Array Coils by Wideband Port Matching. ISMRM. Melbourne, Australia2012. p 2690.
30. Wiggins GC, Brown R, Zhang B, Vester M, Popescu S, Rehner R, Sodickson D. SNR Degradation in Receive Arrays Due to Preamplifier Noise Coupling and a Method for Mitigation. ISMRM. Melbourne, Australia2012. p 2689.

31. Lee RF, Giaquinto R, Constantinides C, Souza S, Weiss RG, Bottomley PA. A broadband phased-array system for direct phosphorus and sodium metabolic MRI on a clinical scanner. Magn Reson Med 2000;43(2):269-277.
32. Schaller BM, Magill AW, Gruetter R. Common modes and cable traps. ISMRM2011. p 4660.
33. Kozlov M, Turner R. Effects of head size and position on SAR. ISMRM. Stockholm, Sweeden2010. p 3875.
34. Wolf S, Diehl D, Gebhardt M, Mallow J, Speck O. SAR simulations for high-field MRI: how much detail, effort, and accuracy is needed? Magn Reson Med 2013;69(4):1157-1168.
35. Ishihara Y, Calderon A, Watanabe H, Okamoto K, Suzuki Y, Kuroda K. A precise and fast temperature mapping using water proton chemical shift. Magn Reson Med 1995;34(6):814-823.